J Mater Sci (2010) 45:5456–5462
DOI 10.1007/s10853-010-4598-x

Luminescence property of $Ca_3(VO_4)_2$:Eu^{3+} dependence on molar ratio of Ca/V and solution combustion synthesis temperature

Kehui Qiu · Junfu Li · Junfeng Li · Xueguang Lu · Yingchun Gong · Junhan Li

Received: 1 September 2009 / Accepted: 4 May 2010 / Published online: 4 June 2010

Abstract Red emitting phosphor $Ca_3(VO_4)_2$:Eu^{3+} was prepared by citric acid-assisted solution combustion method and characterized by X-ray diffraction (XRD), transmission electron microscopy (TEM), and fluorescence spectrophotometer. The influences of Ca to V molar ratio and synthesis temperature on phase composition, morphology, grain size, photofluorescence properties, and ultraviolet–visible diffuse reflectance spectra (UV–Vis DRS) of as-synthesized samples were investigated. The results indicate that Ca to V molar ratio play a key role for the changing of phase composition, excitation spectrum, and luminescence intensity. The sample prepared at 900 °C, keeping Ca/V = 3:2.2, has the highest photoluminescence intensity. The possible causes of the effects on photoluminescence mechanism were also discussed in this work.

Introduction

It is well known that the famous red emission phosphor YVO_4:Eu^{3+} has been widely used in cathode ray tubes (CRT), fluorescent lamps [1, 2], and scintillator in medical image detectors [3]. However, for the high price and rare reserves of Y_2O_3 as raw materials, the utilization of this kind of phosphor is severely restricted. Recently, $Ca_3(VO_4)_2$ and rare earth (Re)-doped calcium orthovanadates (Re = Eu, Sm, Nb, Yb, etc.) artificial crystal materials have attracted increasing interests due to their potential application in solid state lasers [4, 5], luminescent [6], and ferroelectric materials [7], etc. Firstly, calcium is more plenteous and cheaper than yttrium. Secondly, $Ca_3(VO_4)_2$ has many excellent performances, such as the high thermal stabilities, crystallization properties, visible light transmission to be a potential host crystal. More importantly, the luminescence of Eu^{3+} ions can be well sensitized by the isolated VO_4^{3-} group inside $Ca_3(VO_4)_2$ matrix as it does in YVO_4. Hence, $Ca_3(VO_4)_2$:Eu^{3+} may hopefully be a low-cost candidate for YVO_4:Eu^{3+}. These advantages have impelled more and more researchers to study experimental synthesis process and characterization of rare earth-doped $Ca_3(VO_4)_2$ phosphor.

So far, several techniques such as solid state reaction [6, 8–10], co-precipitation [11, 12], hydrothermal [13, 14], sol–gel [15–17], and combustion method [18] etc. have been used to prepare vanadate phosphors. The conventional solid state reaction requires multi-step process including raw material mixture, repeated intermediate grinding, and relatively longer calcination time to obtain pure phase composition as well as high crystallinity degree. This means time-consuming and energy-intensive [19]. However, in solution reaction components can be well-mixed at the molecular level and stoichiometry control [20]. So it is easy to get homogeneous concentrated liquid precursor through a simple processing. In addition, combustion reaction can provide sufficient heat to the system during a short synthesis process. Hence, the solution combustion method turns out to be a good way to synthesize complex compositions with good homogeneity, crystallinity, and high surface area [21]. Considering researches on using sol combustion route to synthesize vanadate-based

K. Qiu (✉) · J. Li · J. Li · X. Lu · Y. Gong · J. Li
Institute of Materials Science and Technology, Chengdu University of Technology, Chengdu 610059, Sichuan, People's Republic of China
e-mail: qkh2188@163.com

J. Li
e-mail: lijunfu1984@163.com

luminescent materials are very limited. This work focuses on employing a citric acid-assisted sol combustion method to synthesize $Ca_3(VO_4)_2$:Eu^{3+} phosphor. The influences of Ca to V molar ratio and synthesis temperature (hereafter termed as T) on the phase composition, fluorescence properties, and ultraviolet–visible diffuse reflectance spectra (UV–Vis DRS) of as-synthesized samples are discussed in detail, and the explanation on luminescence mechanism of this phosphor is also given in the present study.

Experimental

Sample preparation

High purity europium oxide (Eu_2O_3), analytical reagent ammonium metavanadate (NH_4VO_3), calcium nitrate tetrahydrate ($Ca(NO_3)_2{\cdot}4H_2O$), citric acid ($C_6H_8O_7{\cdot}H_2O$), and 2 M nitric acid (HNO_3) were taken as raw materials. The stoichiometric ratio of Eu_2O_3 and $Ca(NO_3)_2{\cdot}4H_2O$, where Eu^{3+} to Ca^{2+} molar ratio is 0.05:0.95, were dissolved in HNO_3 to get mixed solution. Then $C_6H_8O_7{\cdot}H_2O$ and NH_4VO_3 were, respectively, added into the above mixed solution with different molar ratio of Ca to V under stirring and heating at about 70–80 °C. The sol precursor was obtained after stirring for 30 min, which was placed into a furnace preheated at a definite temperature for 1 h in air.

Characterization

The phase composition of as-synthesized samples was checked by X-ray powder diffraction (Philips X'Pert Pro MPD, Cu Kα, 40 kV, 40 mA, $\lambda = 1.5418$ Å). The morphologies and particle sizes were analyzed with a JEM-100CX transmission electron microscopy running at an accelerating voltage of 80 kV. Excitation and emission spectra were measured on Hitachi F-7000 fluorescence spectrophotometer with xenon lamp as excitation source. The UV–Vis diffuse reflectance spectra (UV–Vis DRS) were collected on a Hitachi U-3010 spectrophotometer within the range of 200–800 nm. $BaSO_4$ was used as a reference material. The diffuse reflectance data were then converted to absorbance data using the Kubelka–Munk function:

$$F(R) = \frac{(1-R)^2}{2R} = \frac{K}{S}$$

where R represents the reflectance, while K and S correspond to the effective absorption and scattering, respectively [22]. All the measurements were performed at room temperature.

Results and discussion

Phase compositions

Three samples with different molar ratios of Ca to V from 3:2 to 3:2.5 are synthesized at $T = 900$ °C. Their XRD patterns are depicted in Fig. 1. Sample (a), Ca/V = 3:2, is a mix-phase of $Ca_3(VO_4)_2$ (JCPDS 19-0259) and $Ca_{10}V_6O_{25}$ (JCPDS 52-0649). All diffraction peak positions and the relative intensities of sample (b) are matched well with those of $Ca_3(VO_4)_2$. In the case of sample (c), $Ca_3(VO_4)_2$ is the major phase with a minor of $Ca_2V_2O_7$ (JCPDS 38-0284). It indicates that under the same synthesis temperature (900 °C) pure calcium orthovanadate is obtained as Ca/V = 3:2.2 rather than 3:2 (stoichiometric ratio), but further increase in vanadium will form another impure phase in the product. For the sample (a), if rewritten the molecular formula of $Ca_{10}V_6O_{25}$ as $3x(Ca_3V_2O_8){\cdot}x(CaO)$ ($x = 1$), It could be found that $Ca_{10}V_6O_{25}$ may be formed by a further reaction between superfluous CaO and $Ca_3(VO_4)_2$. From another perspective, the volatilization of V_2O_5, which generated in the prophase of combustion, results in the actual Ca/V < 3:2. That is to say V_2O_5 is easily volatile at 900 °C during the violent combustion processing for its low melting point of 690 °C. However, further increasing the amount of vanadium will make the reaction between $Ca_3(VO_4)_2$ and excessive V_2O_5 come true and lead to the formation of a new phase $2y(Ca_3V_2O_8){\cdot}y(V_2O_5)$, such as $Ca_2V_2O_7$ ($y = 1/3$) as shown in Fig. 1c.

These results reveal that vanadium is easily lost compared with calcium in the combustion process. Hence, pure

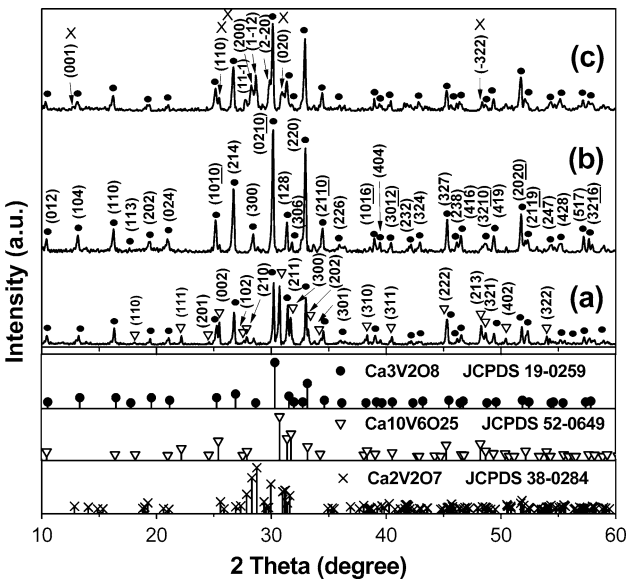

Fig. 1 XRD patterns of the samples prepared at different molar ratios of Ca to V: (*a*) 3:2, (*b*) 3:2.2, and (*c*) 3:2.5, keeping $T = 900$ °C, and the standard patterns of $Ca_3(VO_4)_2$, $Ca_{10}V_6O_{25}$, and $Ca_2V_2O_7$

calcium orthovanadate cannot be synthesized under the condition of sol combustion reaction by mixing reactants followed a strict stoichiometric ratio. In order to prepare pure $Ca_3(VO_4)_2$ phase appropriate adjustment of the Ca to V ratio is necessary to compensate for the volatilization loss of vanadium during combustion reaction process.

Figure 2 presents the XRD patterns of samples prepared at different temperatures with Ca/V = 3:2.2. The diffraction peak positions and the relative intensities of all the samples obtained at three temperatures are matched well with those of the $Ca_3(VO_4)_2$ patterns. No characteristic reflections corresponding to any source materials or impurities are detected in the patterns. This shows that pure $Ca_3(VO_4)_2$ can be obtained at any of the three synthesis temperatures, as long as keeping Ca/V = 3:2.2 constant. With the increase of temperature from 700 to 900 °C, the height of reflections enhance and the Full Width at Half Maximum (FWHM) of diffraction peaks narrow down, for the peak of (02$\underline{1}$0) the FWHM is 0.2260° at 700 °C, 0.2126° at 800 °C, and 0.2118° at 900 °C. The degree of crystallinity and grain diameter increases gradually with the raising of synthesis temperature.

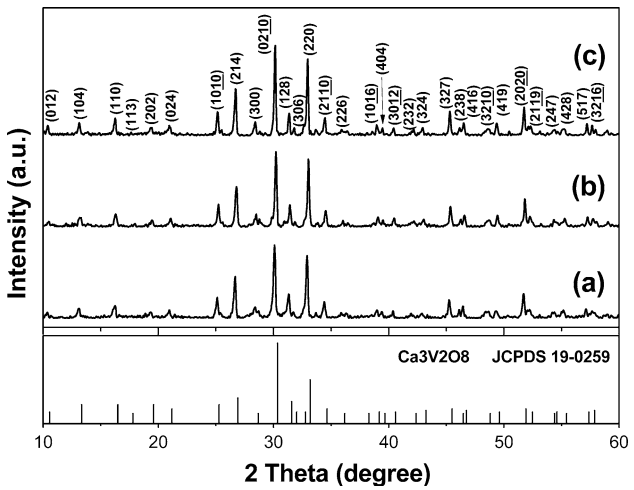

Fig. 2 XRD patterns of the samples, with Ca/V = 3:2.2, prepared at various temperatures: (*a*) 700 °C, (*b*) 800 °C, and (*c*) 900 °C

Morphologies

TEM images in Fig. 3 show the morphologies and the particle sizes of samples obtained at 700 °C (a), 800 °C (b), and 900 °C (c), corresponding to Fig. 2a, b, and c, respectively. The irregular particles are inosculated with each other as shown in Fig. 3a and b. The grain boundaries are vividly visible in Fig. 3b. The particle size of samples is about 30–300 nm at 700 °C, 80–400 nm at 800 °C, and larger than 600 nm at 900 °C. This is consistent with the trend shown in Fig. 2.

Fluorescence properties and UV–Vis absorption spectroscopy

The excitation spectra of samples prepared at different Ca/V, at $T = 900$ °C, exhibit a broad band between 200 and 350 nm with a main peak at 277 nm and a weak shoulder at about 305 nm as shown in Fig. 4. Noticeably, excitation curve of sample (a) splits into two peaks located in 277 and 306 nm with similar intensity. This could be due to the mix-phase of $Ca_3(VO_4)_2$–$Ca_{10}V_6O_{25}$ in sample (a) and the difference of excitation energy between the two phases. In the vanadate phosphors, the excitation band extending from 200 to 350 nm attributes to the absorption of VO_4^{3-} groups in host lattice. The peak at 277 nm and the weak shoulder around 305 nm correspond to the $^1A_1 \rightarrow {}^1T_2$ and $^1A_1 \rightarrow {}^1T_1$ transition [23], respectively, originated from the charge-transfer bands (CTBs) localized within the tetrahedrally coordinated (VO_4^{3-}) group. Another excitation band sprawled from 350 to 475 nm assigns to the *f*–*f* transitions level of Eu^{3+} ions. Three weak peaks at 395, 415, and 465 nm correspond to $^7F_0 \rightarrow {}^5L_6$, $^7F_0 \rightarrow {}^5D_3$ and $^7F_0 \rightarrow {}^5D_2$ transitions, respectively.

In Fig. 5, all the emission properties of samples with various Ca/V characterize the spectroscopy of Eu^{3+} ions. A orange-red emission at 593 nm and a red emission at 613 nm originate from the magnetic dipole transition $^5D_0 \rightarrow {}^7F_1$ and electric dipole transition $^5D_0 \rightarrow {}^7F_2$ of Eu^{3+}, respectively. The other peaks at 557, 655, and 703 nm corresponding to the $^5D_1 \rightarrow {}^7F_2$, $^5D_0 \rightarrow {}^7F_3$, and

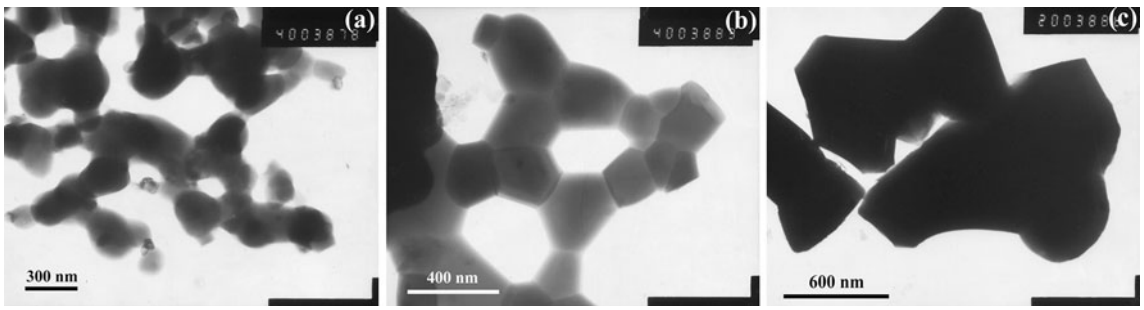

Fig. 3 TEM images of the samples synthesized at different temperatures: **a** 700 °C, **b** 800 °C, and **c** 900 °C, keeping Ca/V = 3:2.2 constant

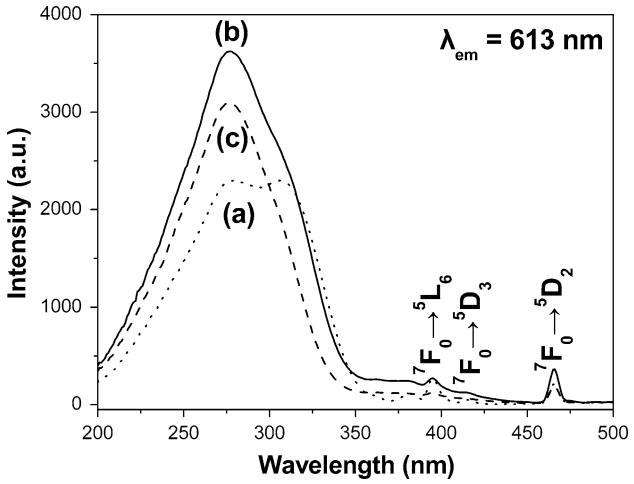

Fig. 4 Excitation spectra of the samples synthesized at different molar ratios of Ca to V: (*a*) 3:2, (*b*) 3:2.2, and (*c*) 3:2.5 keeping $T = 900$ °C constant

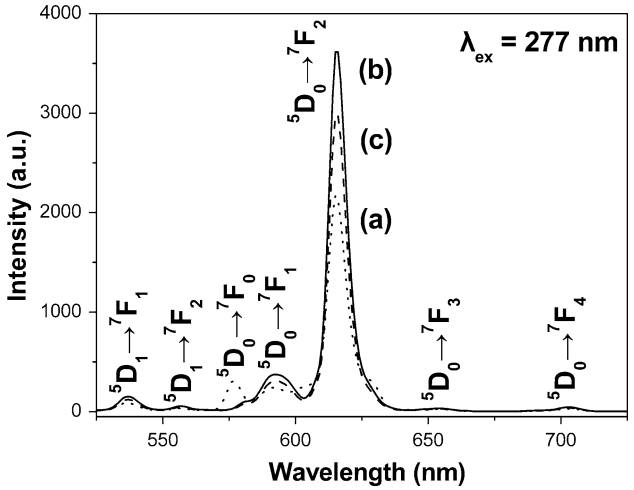

Fig. 5 Emission spectra of the samples synthesized at different molar ratios of Ca to V: (*a*) 3:2, (*b*) 3:2.2, and (*c*) 3:2.5, keeping $T = 900$ °C constant

$^5D_0 \rightarrow {}^7F_4$ transitions are very weak and barely detectable. A relatively high peak at 577 nm may be originated from the $^5D_0 \rightarrow {}^7F_0$ transition of Eu^{3+} ions located in both of $Ca_3(VO_4)_2$ and $Ca_{10}V_6O_{25}$ crystal lattice. Because the radius of Eu^{3+} (1.03 Å) is only slightly larger than that of Ca^{2+} (0.99 Å), Eu^{3+} ion is likely to substitute for Ca^{2+} ion and acts as the luminescence center. Among the transitions of Eu^{3+} originating from $^5D_0$ level, $^5D_0 \rightarrow {}^7F_1$ transition (593 nm) satisfies the magnetic dipole selection rules ($\Delta J = 0, \pm 1$ with $J = 0 \leftarrow/\rightarrow J' = 0$). In free Eu^{3+} ions, however, the $^5D_0 \rightarrow {}^7F_2$ transition (613 nm) is forbidden (for both magnetic and electric dipoles) [24]. According to the Judd–Ofelt theory [25, 26], $^5D_0 \rightarrow {}^7F_2$ transition becomes electric dipole type, due to an admixture of opposite parity $4f^{n-1}5d$ states by an odd parity crystal field component. In the structure of $Ca_3(VO_4)_2$ from Inorganic Crystal Structure Database (ICSD), all of the five Ca^{2+} sites in $Ca_3(VO_4)_2$ are asymmetric, viz. without inversion center. Hence, whichever Ca^{2+} site substituted by the Eu^{3+} ion in $Ca_3(VO_4)_2$, the hypersensitive $^5D_0 \rightarrow {}^7F_2$ ($\Delta J = 2$) transition will be the most prominent one in its emission spectrum. The intensity of the magnetic dipole transition ($^5D_0 \rightarrow {}^7F_1$), hardly changes with the crystal field strength around the Eu^{3+} ion, while the intensity of the hypersensitive electric dipole allowed transition ($^5D_0 \rightarrow {}^7F_2$) is highly sensitive to structural changes and environmental effects in the vicinity of the Eu^{3+} ions [27]. Furthermore, Fig. 5 shows that the height of peak 613 nm is (b) > (c) > (a) and the relative intensities of other weak emission peaks at 537, 557, and 592 nm, etc. are all consonant with the order. As the phase composition varies with the Ca to V ratio, from Ca/V = 3:2 to 3:2.5, $Ca_{10}V_6O_{25}$ forms in sample (a) and $Ca_2V_2O_7$ in sample (c). It indicates that with the changing of V concentration the reaction system undergoes a compositionally induced phase transition that makes a part of Eu^{3+} ions enter into $Ca_{10}V_6O_{25}$ or $Ca_2V_2O_7$ crystal lattice. The crystal field environment around Eu^{3+} ion in these compositions is different. Because the emission properties of Eu^{3+} are dependent upon the neighborhood, such as the symmetry, coordinate environment, V–O–Eu angle, and Eu–O bond length etc. [28]. The changes of emission intensity could be attributed to the structural variations nearby the Eu^{3+} ions. In the present system, Ca^{2+} is the only substitutable ion by Eu^{3+}. There are five types of asymmetric Ca^{2+} sites in $Ca_3(VO_4)_2$ and only two in $Ca_2V_2O_7$ lattice from the ICSD. In $Ca_3(VO_4)_2$, the coordination numbers of two nonequivalent $Ca^{2+}_{(1)}$ cations are 6 and 8, and the other three nonequivalent Ca^{2+} are sixfold, sevenfold, and eightfold coordinated. By contrast, Ca^{2+} cations form in $[Ca_{(1)}O_8]$ and $[Ca_{(2)}O_6]$ asymmetric polyhedra in $Ca_2V_2O_7$ lattice. The minimum and maximum V–O–Ca angles are 98.606° and 154.401° in $Ca_3(VO_4)_2$, 99.274° and 141.406° in $Ca_2V_2O_7$. The average, however, is 122.341° in $Ca_3(VO_4)_2$ and 123.225° in $Ca_2V_2O_7$ indicating that no obvious differences in the tow crystals. Thus, the decreasing of emission intensity with the V concentration changes from Ca/V = 3:2.2 to 3:2.5 may be attributed to the reduction of asymmetric Ca^{2+} site types from $Ca_3(VO_4)_2$ to $Ca_2V_2O_7$. Unfortunately the structure of $Ca_{10}V_6O_{25}$, which is detected in sample (a), is not known. So we made some qualitative explanations by comparing the UV–Vis absorption spectra of host matrix prepared at different Ca/V in later text.

Under different synthesis temperatures from 700 to 900 °C, keeping Ca/V = 3:2.2, samples have similar excitation and emission spectra as shown in Figs. 6 and 7. Spectrum intensity increases in the order of 700, 800, and

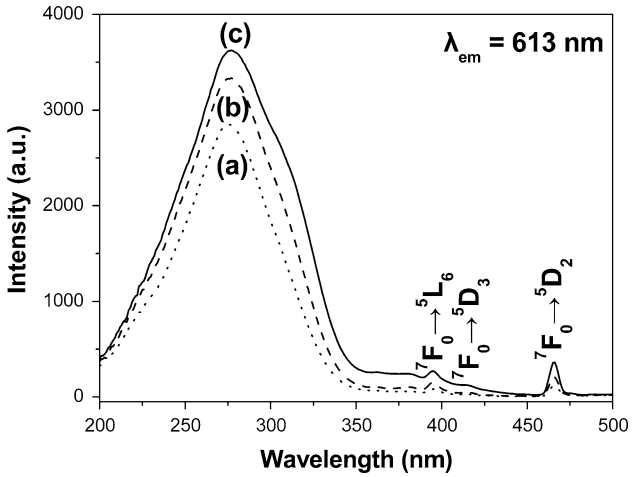

Fig. 6 Excitation spectra of the samples prepared at different temperatures: (*a*) 700 °C, (*b*) 800 °C, and (*c*) 900 °C, keeping Ca/V = 3:2.2 constant

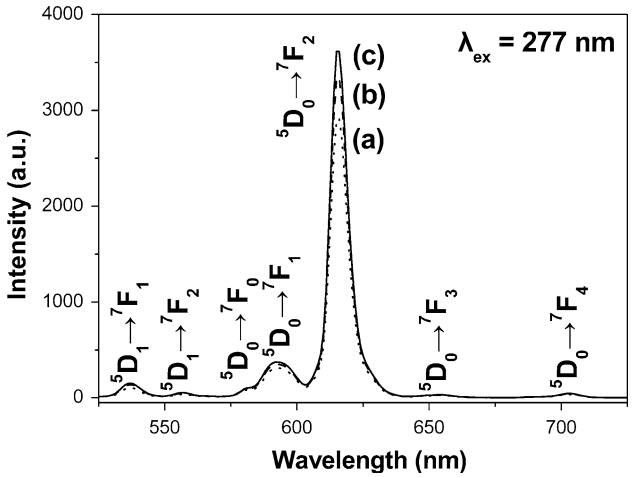

Fig. 7 Emission spectra of the samples prepared at different temperatures: (*a*) 700 °C, (*b*) 800 °C, (*c*) 900 °C, keeping Ca/V = 3:2.2 constant

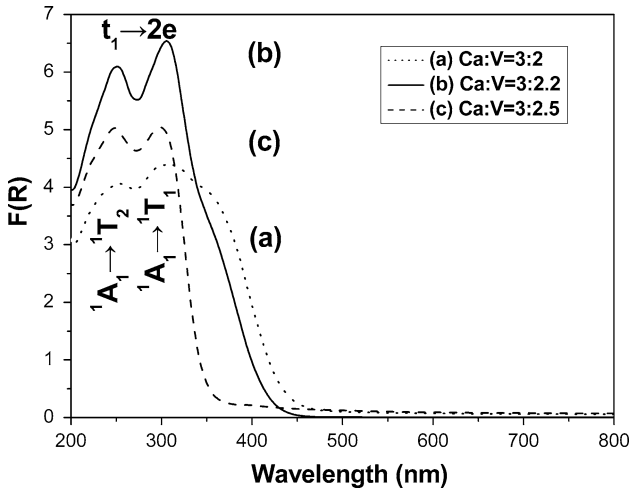

Fig. 8 UV–Vis diffuse reflectance spectra of the samples synthesized at different molar ratios of Ca to V: (*a*) 3:2, (*b*) 3:2.2, and (*c*) 3:2.5, keeping $T = 900$ °C constant

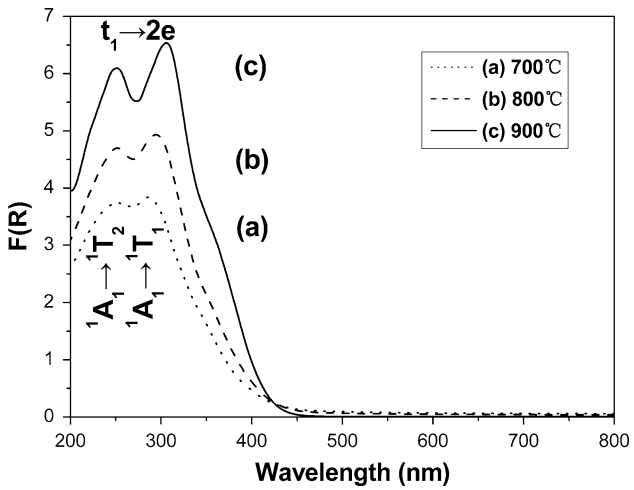

Fig. 9 UV–Vis diffuse reflectance spectra of the samples prepared at different temperatures: (*a*) 700 °C, (*b*) 800 °C, and (*c*) 900 °C, keeping Ca/V = 3:2.2 constant

900 °C. The XRD patterns in Fig. 2 revealed that the crystallization of the single-phase $Ca_3(VO_4)_2$ becomes better and better with the increasing of synthesis temperature. Figure 3 also shows that the crystal grains of $Ca_3(VO_4)_2$ grow larger at higher temperature. At the same time, more Eu^{3+} ions can gain larger kinetic energy to substitute the Ca^{2+} sites and to become luminescence centers, leading to a high energy transfer efficiency from VO_4^{3-} groups to Eu^{3+} ions in $Ca_3(VO_4)_2$. Hence, to some extent, the increasing of the temperature is beneficial for improving the red emission intensity of as-synthesized sample in the conditions of this work.

The UV–Vis absorption spectra of host matrixes prepared at different Ca to V molar ratios and synthesis temperatures are presented in Figs. 8 and 9, respectively. All the compositions show broad absorption band ranging from 200 to 450 nm with two main peaks at about 250 and 305 nm. This band is due to the charge transfer (CT) transition from oxygen to vanadium (O → V). In other words, the electronic transition from the highest occupied molecular orbital (HOMO) primarily O 2p nonbonding orbitals with t_1 symmetry to the lowest unoccupied molecular orbital (LUMO) arises from a linear combination of antibonding V 3d orbitals and O 2p orbitals with e symmetry [29]. The two peaks at about 250 and 305 nm may be assigned to $^1A_1 \rightarrow {}^1T_2$ and $^1A_1 \rightarrow {}^1T_1$ transition [23], respectively.

All the UV–Vis absorption spectral curves as well as their trends show good agreement with the excitation

and emission spectra presented from Figs. 4 to 7. Firstly, from Fig. 8, it can be seen that the sample (b), with Ca/V = 3:2.2, has the highest absorption intensity between 200 and 350 nm compared with sample (a) and sample (c). In terms of the phase analysis in section "Phase compositions", the impurity phase of $Ca_{10}V_6O_{25}$ is found in sample (a) and $Ca_2V_2O_7$ in sample (c). And this may be the direct cause for the decreasing of UV absorption. Secondly, in Fig. 9, under higher synthesis temperature, the $Ca_3(VO_4)_2$ crystal grows more perfect accompanying with the enhancing UV absorption intensity. This means that the absorption and energy transfer between VO_4^{3-} groups and Eu^{3+} ions in $Ca_3(VO_4)_2$ become more efficient, which make as-synthesized samples exhibit higher excitation and emission intensity as shown in Figs. 6 and 7.

The luminescence mechanism of $Ca_3(VO_4)_2$:Eu^{3+} phosphor can be depicted using Fig. 10. It is a combine action of host sensitizing and the radiative transition of Eu^{3+} ions. $Ca_3(VO_4)_2$:Eu^{3+} is a typical host sensitizing luminescence material. Its emission intensity and efficiency mainly depend on the host absorption and energy transfer from the host to activators [30]. Once UV photons are absorbed by the host matrix, the center V^{5+} ions of VO_4^{3-} groups are excited from the ground state ($^1A_1$) to the excited state ($^1T_1$, $^1T_2$). Thereafter, the absorption of UV photons by the VO_4^{3-} groups inside the host is followed by a non-radiative transfer to Eu^{3+} and then the VO_4^{3-} groups return to the singlet ($^1A_1$) state from the triplet ($^3T_1$, $^3T_2$). The triplet ($^3T_1$, $^3T_2$) → singlet ($^1A_1$) transition connects to a transfer of an electron from a molecular orbital mainly localized on one oxygen atom (2pπ type) to a molecular orbital mainly localized on the vanadium atom (d_e or d_{t_2} type) [31]. Meanwhile the excited Eu^{3+} comes back to the ground state through a red radiative transition and emits its characteristic radiation [32]. The five emission lines of $Ca_3(VO_4)_2$:Eu^{3+} at about 703, 655, 613, 593, and 581 nm (in Figs. 5, 7) are assigned to the transitions from the metastable orbital singlet state $^5D_0$ to the spin–orbit states ^7F_J (J = 0, 1, 2, 3, 4) of Eu^{3+} [33, 34]. Based on the results and discussions in the present study, Ca to V molar ratio and synthesis temperature mainly bring two facets of influences on the above photoluminescence process of $Ca_3(VO_4)_2$:Eu^{3+} phosphor. (1) Effects on the UV radiation absorption efficiency (η_A shown in Fig. 10) of system. With the changing of Ca to V molar ratio from 3:2 to 3:2.5, the host matrix undergoes a compositionally induced phase transition. As Ca/V = 3:2 (Fig. 1a), the sample contains $Ca_{10}V_6O_{25}$ impurity phase, while, as Ca/V = 3:2.5 (Fig. 1c), $Ca_2V_2O_7$ phase is detected. This structural change leads to the decreasing of UV absorption efficiency of sample (a) and (c). (2) Influences on the energy transfer process from VO_4^{3-} groups to Eu^{3+} ions. With the increasing of synthesis temperature the crystallization of host matrix becomes more complete. Thus, higher energy transfer efficiency (η_{ET}) can be achieved in the perfect crystal framework. Besides, the structural difference of $Ca_3(VO_4)_2$, $Ca_2V_2O_7$, and $Ca_{10}V_6O_{25}$ will also change the η_{ET} from VO_4^{3-} groups to Eu^{3+} ions. All of these factors can affect the red emission intensity of $Ca_3(VO_4)_2$:Eu^{3+} phosphor in different degrees.

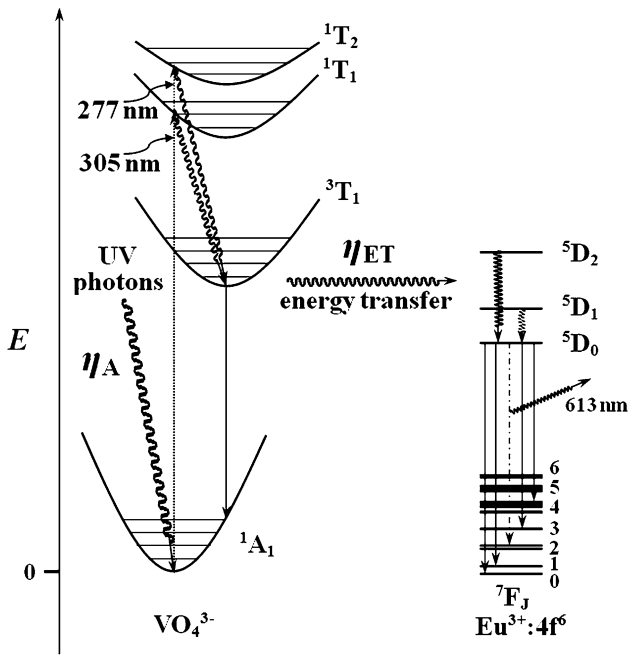

Fig. 10 Energy transfer process from VO_4^{3-} to Eu^{3+} in $Ca_3(VO_4)_2$

Conclusions

The results obtained from the above will be summarized as below.

(1) $Ca_3(VO_4)_2$:Eu^{3+} red emission phosphor is successfully synthesized by a new sol combustion process. The X-ray diffraction and fluorescence spectrophotometer results indicate that pure and highly effective $Ca_3(VO_4)_2$:Eu^{3+} red emitting powders can be obtained through this route.

(2) The molar ratio of calcium to vanadium is a key factor for the phase composition of samples, which affects the fluorescence properties of phosphor evidently. The existence of impurity phases will decrease the ultraviolet absorption efficiency of host matrix and the energy transfer efficiency from VO_4^{3-} groups to Eu^{3+} ions, leading to a low excitation and emission intensities of phosphors. The optimum molar ratio of Ca to V is 3:2.2 to obtain pure $Ca_3(VO_4)_2$ phase.

(3) The emission intensity of $Ca_3(VO_4)_2$:Eu^{3+} phosphor increases with the raising of the synthesis temperature

from 700 to 900 °C. The sample synthesized at 900 °C as Ca/V = 3:2.2 is endued with the highest emission intensity in the conditions of this work.

Acknowledgements This work is supported by the Key Scientific and Technological Research and Development Program (Grant No. 07GG002-002), The Natural Science Foundation (Grant No. 08GY0082), and the Nature Science Foundation of the Panzhihua City (Grant No. 2009CY-C-4) in Sichuan Province, P.R. China.

References

1. Riwotzki K, Haase M (2001) J Phys Chem B 105:12709. doi:10.1021/jp0113735
2. Osvaldo AS, Simone AC, Renata RI (2000) J Alloys Compd 303–304:316. doi:10.1016/S0925-8388(00)00595-8
3. Panayiotakis G, Cavouras D, Kandarakis I, Nomicos C (1996) Appl Phys A 62:483. doi:10.1007/BF01567121
4. Brixner LH, Flournoy PA (1965) J Electrochem Soc 112:303. doi:10.1149/1.2423528
5. Andrade LHC, Reyes Ardila D, Andreeta JP, Siu Li M (2003) Opt Mater 22:369. doi:10.1016/S0925-3467(02)00371-3
6. Grzechnik A, Mcmillan PF (1997) J Solid State Chem 132:156. doi:10.1006/jssc.1997.7435
7. Glass AM, Abrahams SC, Ballman AA, Loiacono G (1978) Ferroelectrics 17:579. doi:10.1080/00150197808236782
8. Lee SS, Kim HJ, Byeon SH, Park JC, Kim DK (2005) Ind Eng Chem Res 44:4300. doi:10.1021/ie048953j
9. Ding WJ, Wang J, Zhang M, Zhang QH, Su Q (2006) J Solid State Chem 179:3582. doi:10.1016/j.jssc.2006.07.007
10. Su MZ, Zhou J (1994) J Alloys Compd 207–208:406. doi:10.1016/0925-8388(94)90250-X
11. Yan B, Su XQ (2007) J Alloys Compd 431:342. doi:10.1016/j.jallcom.2006.05.095
12. Yan B, Su XQ (2007) Optical Mater 29:1866. doi:10.1016/j.optmat.2006.10.024
13. Forbes AR, McMillen CD, Giesber HG, Kolis JW (2008) J Crystal Growth 310:4472. doi:10.1016/j.jcrysgro.2008.06.067
14. Wu JH, Yan B (2008) J Alloys Compd 455:485. doi:10.1016/j.jallcom.2007.01.162
15. Yu M, Lin J, Wang Z, Fu J, Wang S, Zhang HJ, Han YC (2002) Chem Mater 14:2224. doi:10.1021/cm011663y
16. Zhang J, Zhang Z, Tang Z, Tao Y, Long X (2002) Chem Mater 14:3005. doi:10.1021/cm011744u
17. Li J, Kuwabara M (2003) Sci Technol Adv Mater 4:143. doi:10.1016/S1468-6996(03)00027-5
18. Zhang HP, Lü MK, Yang ZS, Xiu ZL, Zhou GJ, Wang SF, Zhou YY, Wang SM (2006) J Alloys Compd 426:384. doi:10.1016/j.jallcom.2006.02.028
19. Cousin P, Ross RA (1990) Mater Sci Eng A 130:119. doi:10.1016/0921-5093(90)90087-J
20. Wang X, Chen XY, Gao LS, Zheng HG, Ji MR, Shen T, Zhang ZD (2003) J Crystal Growth 256:123. doi:10.1016/S0022-0248(03)01289-2
21. Van Landschoot N, Kelder EM, Schoonman J (2004) Solid State Ionics 166:307. doi:10.1016/j.ssi.2003.11.006
22. Kubelka P, Munk F (1931) Z Tech Phys 12:593–601
23. Blasse G (2006) The luminescence of closed-shell transition-metal complexes. new developments. In: Luminescence and energy transfer. Springer-Verlag, Berlin, pp 1–41
24. Ray S, Pramanik P, Singha A, Roy A (2005) J Appl Phys 97(9): 094312. doi:10.1063/1.1884759
25. Judd BR (1962) Phys Rev 127(3):750. doi:10.1103/PhysRev.127.750
26. Ofelt GS (1962) J Chem Phys 37(3):511. doi:10.1063/1.1701366
27. Yu M, Lin J, Fang J (2005) Chem Mater 17(7):1783. doi:10.1021/cm0479537
28. Blasse G (1966) J Chem Phys 45(7):2356. doi:10.1063/1.1727946
29. Dolgos MR, Paraskos AM, Stoltzfus MW, Yarnell SC, Woodward PM (2009) J.Solid State Chem 182:1964. doi:10.1016/j.jssc.2009.04.032
30. Liu B, Shi CS, Zhang QL (2002) J Alloys Compd 333:215. doi:10.1016/S0925-8388(01)01711-X
31. Belletti A, Borromei R, Cavalli E, Oleari L (1998) Eur J Solid State Inorg Chem 35:483. doi:10.1016/S0992-4361(98)80025-8
32. Yu YQ, Zhou SH, Zhang SY (2003) J Alloys Compd 351:84. doi:10.1016/S0925-8388(02)01031-9
33. Haase M, Riwotzki K, Meyssamy H, Kornowski A (2000) J Alloys Compd 303–304:191. doi:10.1016/S0925-8388(00)00628-9
34. Huignard A, Buissette V, Franville A-C (2003) J Phys Chem B 107:6754. doi:10.1021/jp0342226